Acta Biochim Biophys Sin 2022, 54(7): 961–973
https://doi.org/10.3724/abbs.2022081
Advance Access Publication Date: 18 July 2022
Original Article

Original Article

miR-335-5p regulates the proliferation, migration and phenotypic switching of vascular smooth muscle cells in aortic dissection by directly regulating SP1

Runwei Ma[1,*], Dayong Zhang[2], Yi Song[3], Jichang Kong[1], Chunjie Mu[1], Pin Shen[1], and Wenting Gui[3]

[1]Department of Cardiovascular Surgery, Fuwai Yunnan Cardiovascular Hospital, Kunming 650102, China, [2]Department of Cardiovascular Surgery, Guangyuan Central Hospital, Guangyuan 628099, China, and [3]Department of Extracorporeal Circulation, Fuwai Yunnan Cardiovascular Hospital, Kunming 650102, China
*Correspondence address. Tel: +86-871-6852685; E-mail: marw0102@163.com

Received 5 November 2021 Accepted 13 December 2021

Abstract
Uncontrolled proliferation, migration and phenotypic switching of vascular smooth muscle cells (VSMCs) are important steps in the development and progression of aortic dissection (AD). The function and potential mechanism of miR-335-5p in the pathogenesis of AD are explored in this study. Specifically, the biological function of miR-335-5p is explored *in vitro* through CCK-8, Transwell, immunofluorescence, EdU, wound-healing, RT-qPCR and western blotting assays. In addition, an AD model induced by angiotensin II is used to investigate the function of miR-335-5p *in vivo*. A dual-luciferase assay is performed to verify the targeting relationship between miR-335-5p and specificity protein 1 (SP1). Experiments involving the loss of SP1 function are performed to demonstrate the function of SP1 in the miR-335-5p-mediated regulation of human aortic-VSMCs (HA-VSMCs). AD tissues and platelet-derived growth factor BB (PDGF-BB)-stimulated HA-VSMCs show significant downregulation of miR-335-5p expression and upregulated SP1 expression. Overexpression of miR-335-5p effectively suppresses cell proliferation, migration and synthetic phenotype markers and enhances contractile phenotype markers induced by PDGF-BB treatment. Additionally, SP1 is identified as a target gene downstream of miR-335-5p, and its expression is negatively correlated with miR-335-5p in AD. Upregulation of SP1 partially reverses the inhibitory effect of miR-335-5p on HA-VSMCs, whereas the downregulation of SP1 has the opposite effect. Furthermore, Ad-miR-335-5p clearly suppresses aorta dilatation and vascular media degeneration in the AD model. Our results suggest that miR-335-5p inhibits HA-VSMC proliferation, migration and phenotypic switching by negatively regulating SP1, and indicate that miR-335-5p may be a potential therapeutic target in AD.

Key words aortic dissection, miR-335-5p, phenotypic switch, vascular smooth muscle cells

Introduction

The normal aortic wall is divided into three layers: intima, media and adventitia. Due to a variety of internal or external factors caused by acute damage to the intima of the aorta, high-speed blood flow through the tear into the aorta between the intima and media forms a false cavity, which is called aortic dissection (AD) [1–3]. If the cavity ruptures, the patient will suffer from cardiac arrest at any time. AD, which is a cardiovascular emergency that seriously endangers human life, exhibits rapid onset and high morbidity and fatality rates. Without immediate surgical intervention, the fatality rate of acute AD can reach 50%–68% within 48 h and up to 90% within 3 months after occurrence [4,5]. With the recent development of medical diagnosis technology, the diagnosis of this disease is no longer a major problem, but the effective treatment of AD remains a challenge. Further exploration of the pathogenesis of AD is conducive to the development of new drugs and prevention of its progression.

In patients with AD, the aortic medial membrane is often characterized by apoptosis of smooth muscle cells, degenerative chan-

© The Author(s) 2022. This is an open access article distributed under the terms of the Creative Commons Attribution Non-Commercial License (https://creativecommons.org/licenses/by-nc/4.0/).

ges in the extracellular matrix, rupture of elastic fibers, and intracellular accumulation of proteoglycans and glycosaminoglycans, and these effects lead to decreased elasticity and vulnerability of the aortic wall [6]. Blood vessels are composed of the intima, media and adventitia [7], and their main cellular components are endothelial cells, smooth muscle cells and fibroblasts. Vascular endothelial cells and smooth muscle cells (VSMCs) play an important role in maintenance of the normal physiological functions of blood vessels in the development of cardiovascular diseases [8,9]. VSMCs have the ability to differentiate [10], and as the number of replications increases, VSMCs undergo phenotypic switching, which reduces the expression of functional markers such as smooth muscle 22 α (SM22α), smooth muscle cell-specific myosin heavy chain (MYH11), and α smooth muscle actin (α-SMA), and enhances cell proliferation, migration and secretion [11,12]. The phenotypic switching of VSMCs from a contractile phenotype to a synthetic phenotype might be involved in the development of thoracic aortic aneurysms and dissection [13–16]. However, the molecular mechanism underlying the phenotypic switching of VSMCs in AD is not well understood. Therefore, further study of the biological behavior and regulatory mechanism of VSMCs is important for providing new directions and new targets for the prevention and treatment of cardiovascular and cerebrovascular diseases.

MicroRNAs (miRNAs) are a class of single-stranded noncoding RNAs with lengths of 19–21 bp that widely exist in the biological world [17,18]. miRNAs can specifically recognize the 3′-untranslated region (3′-UTR) of the target gene mRNA, inhibit the translation of the target gene or promote its degradation, and subsequently regulate the expression of the target gene [19,20]. A variety of miRNAs have been found to be associated with some cardiovascular diseases, such as cardiac hypertrophy, atherosclerosis and neointima formation [18]. miRNAs are involved in various pathological processes of cardiovascular diseases and play a key role in the development of the cardiovascular system and diseases. AD is a serious cardiovascular disease, and some researchers have found that miRNAs are significantly differentially expressed in the tissues of patients with AD through gene microarray studies and hope to reveal the potential role of miRNAs in the pathogenesis of AD [21–23]. The upregulation of miR-335-5p represses esophageal squamous cell carcinoma (ESCC) progression [24]. miR-335 may be a potential therapeutic target in cardiac fibrosis and hypertrophy because this miRNA is downregulated in the heart tissues of angiotensin II-induced mice and an angiotensin II-stimulated mouse cardiomyocyte cell line [25]. miR-335 can strongly halt the effects of classical inflammatory stimuli in both microglia and neuronal cells and thus attenuate chronic neuroinflammation [26]. In addition, miR-335 is involved in the progression of acute myeloid leukemia, ovarian cancer and colorectal liver metastases [27–29]. However, the function of miR-335-5p in AD and its potential mechanism remain to be identified.

Specificity protein 1 (SP1) was first discovered by Dynan *et al.* [30] in the promoter of simian virus 40 and was the first transcription factor isolated and purified from mammals. SP1 belongs to the specificity protein/Krüppel-like factor family and is an important regulator of multiple cell events, such as the cell cycle, proliferation, and apoptosis [31,32]. The level of SP1 increases during the development of ischemia/reperfusion [33,34], Parkinson's disease [35,36] and Alzheimer's disease [37]. SP1 is involved in VSMC proliferation and phenotype switching [38], which indicates that SP1 may be involved in the development of AD.

In our study, we aimed to confirm whether miR-335-5p suppresses the proliferation and phenotypic switching of human aortic-VSMCs (HA-VSMCs) by directly downregulating SP1 during the pathophysiological processes of AD. We found that miR-335-5p expression in the AD group was markedly lower than that in the normal group and that the miR-335-5p mimic inhibited the proliferation, migration and phenotypic switching of HA-VSMCs induced by platelet-derived growth factor BB (PDGF-BB). Furthermore, a negative correlation was found between miR-335-5p and SP1 expression *in vivo*, and the expression of SP1 was modulated by transfection with the miR-335-5p mimic *in vitro*, which suggested the involvement of miR-335-5p in the development of AD through the negative regulation of SP1. In addition, the upregulation of miR-335-5p clearly suppressed aorta dilatation and vascular media degeneration in a mouse model of AD induced by angiotensin II. These findings might provide insights into the effect of miR-335-5p in regulating the function of HA-VSMCs in AD at the molecular level.

Materials and Methods

Tissue samples

All tissue samples (AD tissues, $n = 36$; normal tissues, $n = 19$) used in this study were collected at the Fuwai Yunnan Cardiovascular Hospital from February 2019 to March 2020. The AD samples were collected from patients who were diagnosed with AD through pathological examination and who did not receive any radiotherapy or chemotherapy prior to surgery. Normal aorta samples were harvested from age- and sex-matched patients undergoing valve replacement. Among the collected samples, 6 AD and 4 normal samples were used in the miRNA microarray analysis, 10 AD and 10 normal samples were utilized in the real-time quantitative PCR (RT-qPCR) validation assay and eight of the 10 samples were also used for the western blot assay, 5 AD and 5 normal samples were used for hematoxylin and eosin (H&E) staining, and 15 AD tissues were used for the correlation analysis. Written informed consents were obtained from all the participants. The study was approved by the Ethics Committee of Fuwai Yunnan Cardiovascular Hospital (2020-032-01). All animal experiments were approved by the Animal Ethics Committee of Kunming Medical University (kmmu2021433).

miRNA-seq analysis

Six AD samples and 4 normal samples were used in the miRNA microarray analysis. miRNAs from tissues were extracted using an RNAmisi microRNA kit (RN0501; Aidlab Biotechnologies, Beijing, China) according to the manufacturer's protocol. The miRNA expression profile of aortic tissues was analyzed by Majorbio Biomedical Technology (Shanghai, China). The reference genome used to analyze our miRNA-seq data was Homo sapiens version GRCh38.p13 from http://asia.ensembl.org/Homo_sapiens/Info/Index. The raw data were normalized, and the basic analysis was performed using Genespring GX 12.5 software (Agilent Technologies, Santa Clara, USA). DESeq2 was subsequently used to determine the false discovery rate (FDR) threshold (adjusted *P* value). The differentially expressed genes (DEGs) with an adjusted *P* value ≤ 0.05 and $|\log_2^{FC}| \geq 1$ (FC, fold change) were used to identify the number of DEGs in the different groups.

Cell culture and plasmids

HA-VSMCs, which were purchased from CHI Scientific (Jiangyin,

China), were cultured in DMEM/F12 (Invitrogen, Carlsbad, USA) supplemented with 10% FBS, 100 U/ml penicillin, and 100 μg/ml streptomycin in a humidified atmosphere with 5% CO_2 at 37°C. The cells were used at passage 3–6. SP1 target oligo (5′-CTGCCGTTGG CTATAGCAAAT-3′) and negative control (NC) oligo (5′-TTC TCCGAACGTGTCACGT-3′) were synthesized and inserted into the pGPH1/Neo-shRNA vector by GenePharm (Shanghai, China). The SP1 cDNA sequences were inserted into the pcDNA3.1 vector with *Bam*HI and *Xho*I enzyme sites by GenePharm. The hsa-miR-335-5p mimic (5′-UCAAGAGCAAUAACGAAAAAUGU-3′) and NC mimic (5′-UUCUCCGAACGUGUCACGUTT-3′) were purchased from GenePharm.

CCK-8 (cell counting kit-8) assay

HA-VSMCs were seeded on 96-well plates at a density of 2×10^4 cells/well, incubated for 24 h at 37°C and then transfected or cotransfected with the miR-335-5p mimic or NC mimic, SP1/pcDNA3.1 or pcDNA3.1 and SP1/pGPH1 or pGPH1 using Lipofectamine 2000 (Invitrogen) according to the manufacturer's protocol for 24 h. The cells were then treated or not treated with PDGF-BB (20 ng/mL; PeproTech, Rocky Hill, USA) for 24, 48, and 72 h at 37°C. Subsequently, 20 μL of CCK-8 solution (C0037; Beyotime, Shanghai, China) was added to each well, and the plates were incubated for 4 h at 37°C. The absorbance (OD 450 nm) was observed and measured using a Tecan Infinite M1000 microplate reader (Tecan Company, Männedorf, Switzerland).

EdU (5-ethynyl-2′-deoxyuridine) assay

HA-VSMCs were seeded into a 6-well plate and then transfected or cotransfected with miR-335-5p mimic or NC mimic, SP1/pcDNA3.1 or pcDNA3.1 and SP1/pGPH1 or pGPH1 using Lipofectamine 2000 according to the manufacturer's protocol for 24 h. The cells were then treated or not treated with PDGF-BB (20 ng/mL; PeproTech) for 24 h at 37°C and then incubated with BeyoClick™ EdU-594 (C0078S; Beyotime) diluted at 1:500 for 2 h at 37°C. Subsequently, the cells were fixed with 4% paraformaldehyde for 15 min, subjected to three 5-min washes with PBS and incubated with PBST (PBS containing 0.3% Triton X-100) for 15 min at room temperature. The cells were then incubated with 500 μL of Click Additive Solution in the dark for 30 min at room temperature and then subject to three 5-min washes with PBST at room temperature. The cell nuclei were stained with DAPI (C1005; Beyotime) and the cells were observed under a TE2000-U fluorescence microscope (Nikon, Tokyo, Japan). The EdU-positive cells in 6 visual fields were detected and counted.

Wound-healing assay

HA-VSMCs were seeded into a 6-well plate and then transfected or cotransfected with miR-335-5p mimic or NC mimic, SP1/pcDNA3.1 or pcDNA3.1 and SP1/pGPH1 or pGPH1 using Lipofectamine 2000 according to the manufacturer's protocol for 24 h. A linear scratch was then rapidly made using a 200-μL pipette tip in the center of a dish, and the cells were treated or not treated with PDGF-BB (20 ng/mL) for 24 h at 37°C. Images of the migrated cells were captured with the TE2000-U fluorescence microscope. The migrated distances were calculated, and the average was calculated for statistical analysis.

Migration assay

HA-VSMCs were seeded into a 6-well plate at a density of 8×10^4 cells/well, incubated overnight, and then transfected with miR-335-5p mimic or NC mimic, SP1/pcDNA3.1 or pcDNA3.1 and SP1/pGPH1 or pGPH1 using Lipofectamine 2000 according to the manufacturer's protocol for 24 h. The cells were then collected using 0.25% trypsin (Gibco, New York, USA) and resuspended in 1 mL of serum-free medium. Subsequently, 200 μL of cell solution (2×10^4 cells) was added to each upper chamber of the Transwell (8-μm pores; Corning, New York, USA), and 500 μL of complete medium was added to the lower chamber. The cells were treated or not treated with PDGF-BB (20 ng/mL) for 24 h at 37°C. The cells that migrated to the lower surface of the Transwell were fixed with 70% methanol, stained with 0.5% crystal violet solution and then imaged under the TE2000-U fluorescence microscope (magnification, × 200). Five independent visual fields in each well of migrated cells were photographed and counted, and the average number was calculated.

Stress fiber (F-actin) staining

HA-VSMCs were seeded into a 6-well plate and then transfected with miR-335-5p mimic or NC mimic, SP1/pcDNA3.1 or pcDNA3.1 and SP1/pGPH1 or pGPH1 using Lipofectamine 2000 according to the manufacturer's protocol for 24 h. The cells were then treated or not treated with PDGF-BB (20 ng/mL) for 24 h at 37°C. The cells were washed with PBS and fixed with 4% formaldehyde in 6-well dishes for 20 min at room temperature. The cells were subjected to three 5-min washes with PBST (PBS containing 0.1% Triton X-100) at room temperature and incubated with Actin-Tracker Green-488 (1:200, C2201S; Beyotime) in the dark for 1 h at 4°C. The cell nuclei were stained with DAPI (C1005; Beyotime) and the cells were subjected to three 5-min washes with PBST at room temperature. Fluorescence images were obtained under the TE2000-U fluorescence microscope. The average integral optical density of the stress fibers in 6 visual fields was quantified using ImageJ 2x software (National Institutes of Health, Bethesda, USA).

Construction of AD model

Eighteen 8- to 10-week-old female $ApoE^{-/-}$ mice were purchased from Vital River Company (Beijing, China) and randomly divided into three groups ($n = 6$ in each group): normal group, AD group and Ad-miR-335-5p group. All animal experiments were performed in accordance with the guidelines of the Laboratory Animal Centre of Kunming Medical University. Twelve $ApoE^{-/-}$ mice were treated with angiotensin II (injected intraperitoneally, 20 mg/kg/day; Sangon, Shanghai, China) and fed with a 21% high-fat diet (Vital River) for 4 weeks to construct the AD model. And 1, 2, and 3 weeks after initiation of the construction of the AD model, the $ApoE^{-/-}$ mice in the AD and Ad-miR-335-5p groups were injected with 20 μL of Ad-NC or Ad-miR-335-5p (10^{10} pfu/mL; GeneChem, Shanghai, China) around the thoracic aorta arch. After model construction, the mice were euthanized with 150 mg/kg pentobarbital sodium via intraperitoneal injection. The aortas were harvested for H&E and immunohistochemical assays.

Dual-luciferase reporter assay

SP1 DNA sequences consisting of 300 bp around the miR-335-5p wild-type (WT) binding site or mutant (MUT) site were synthesized and inserted into the psiCHECK2 vector following the luciferase gene using the *Pme*I and *Xho*I enzyme sites by GenePharm. HA-VSMCs were transfected in 12-well plates with 0.5 μg of psiCHECK2

reporter vectors (Promega, Madison, USA) (empty, SP1-WT 3′-UTR, SP1-MUT 3′-UTR) and miR-335-5p or NC mimic (20 nM) according to the instructions provided with the Dual-luciferase Reporter Assay System (E1910; Promega). The relative luciferase activity was normalized to Renilla activity using the Tecan Infinite M1000 microplate reader.

Real-time quantitative PCR (RT-qPCR) assay

Total RNA from tissues and cells was isolated using TRIzol reagent (15596018; Invitrogen) according to the manufacturer's protocol. miRNAs from the cells were extracted using an RNAmisi microRNA kit (RN0501; Aidlab) according to the manufacturer's protocol. First-strand cDNA was generated from total RNAs and miRNAs using the PrimeScript RT Reagent Kit (RR036Q; Takara, Dalian, China) and the miRNA first-strand synthesis kit (PC4801; Aidlab), respectively, according to the manufacturer's instructions. Real-time PCR was performed using SYBR Green Premix (RR420A; Takara) or miRNA qPCR Mix (PC6301; Aidlab) and an ABI 7900 real-time PCR system (Applied Biosystems, Foster City, USA). The results were analyzed using the $2^{-\Delta\Delta Ct}$ method. *GAPDH* and *U6* served as the internal controls for the mRNA and miRNA qPCR assays, respectively. The primer sequences used are listed in Table 1.

Western blot analysis

The cells were lysed using RIPA lysis buffer (P0013B; Beyotime) for total protein extraction. The proteins were quantified using a BCA kit (P0012; Beyotime), separated by 10% SDS-PAGE (P0012A; Beyotime), and transferred onto 0.45-μm polyvinylidene fluoride (PVDF) membranes (IPVH00010; Millipore, Billerica, USA). The membranes were blocked with 5% nonfat milk (P0216; Beyotime) for 2 h at room temperature and then incubated with primary antibodies against α-SMA (1:1000, bs-10196R; Bioss, Beijing, China), SM22α (1:1000, 10493-1-AP; ProteinTech, Rosemont, USA), CNN1 (1:1000, bs-0095R; Bioss), OPN (1:1000, bs-0026R; Bioss), Collagen I (1:1000, 14695-1-AP; ProteinTech) and β-actin (1:2000, 20536-1-AP; ProteinTech) overnight at 4°C. The membranes were then incubated with goat anti-rabbit IgG (1:5000, SA00001-2; ProteinTech) at 37°C for 1 h. An ECL chemiluminescence kit (P0018S; Beyotime Institute of Biotechnology) was utilized for chemiluminescence detection with the Bio-Rad Gel Doc XR$^+$ Gel Imaging System (Bio-Rad, Hercules, USA). β-Actin served as an internal control. ImageJ 2x software was used to quantify the protein bands.

Hematoxylin and eosin (H&E) staining

The tissues were fixed with 4% paraformaldehyde and then embedded in paraffin using routine methods. Four-micrometer-thick tissue sections were cut and then subjected to xylene dewaxing and gradient alcohol (100%, 95%, 90%, 80%, and 70% ethanol) rehydration. The paraffin-embedded samples were cut into 4-μm-thick slices and placed on slides. The slides were dewaxed, hydrated, and stained using an H&E Staining Kit (G1120; Solarbio, Beijing, China) according to the instructions. The slides were then dehydrated with ethanol, cleared with xylene, sealed with neutral gum, and visualized using an optical microscope (ECLIPSE Ci; Nikon) under different magnifications to confirm the formation of AD. All slides were observed by a blinded investigator under the ECLIPSE Ci microscope (200×). Five fields of each slice were selected, and the aortic media thickness was measured using ImageJ 2x software.

Immunohistochemical staining

The 4-μm-thick sections were deparaffinized in xylene and hydrated using an ethanol-deionized water series. The sections were incubated with 3% H_2O_2 for 10 min at room temperature to block endogenous peroxidase activity, blocked with 5% goat serum (Solarbio), and then incubated with anti-SP1 antibody (1:200, bs-0975R; Bioss), anti-α-SMA antibody (1:200, bs-10196R; Bioss) and anti-OPN antibody (1:200, bs-0026R; Bioss) at 4°C overnight and then with HRP-labeled secondary antibody (1:500, AS014; ABclonal, Wuhan, China) at room temperature for 1 h. The sections were stained with a DAB kit (Maixin, Fuzhou, China) according to the manufacturer's instructions. The sections were then counterstained with hematoxylin for 5 min at room temperature to visualize the nuclei and observed under the ECLIPSE Ci microscope (magnification × 400). Brownish-yellow granules indicate immunoreactive (positive) cells, and the levels of positive protein expression were quantified using ImageJ 2x software.

Statistical analysis

GraphPad Prism 5.0 software (GraphPad Software, San Diego, USA) was used for the statistical analyses. Data are expressed as the mean ± standard deviation (SD). Each experiment was performed at least three times independently. The differences between two groups were compared by Student's *t*-test (two-tailed) and the differences among three or more groups were assessed by one-way ANOVA with Tukey's post-hoc test. $P < 0.05$ was considered to indicate statistical significance.

Results

miR-335-5p is downregulated in AD tissue

miRNA sequencing analyses of 6 dissected aortic tissues and 4 normal aortic tissues were performed, and the dissected and normal human aortic tissues were subject to H&E staining. As demonstrated by the staining analysis, the normal aortic tissue showed a complete and continuous aortic structure (intima, tunica media and adventitia), and the VSMCs in the normal group exhibited a normal morphology and were well aligned. In contrast, the AD group exhibited separation between the intima and tunica media, substantial vascular media degeneration with disordered filament assembly, and larger and more rounded VSMCs (Figure 1A). A total of 23 differentially expressed miRNAs were obtained, including 18 upregulated and 5 (miR-335-5p, miR-335-3p, miR-203a-3p, miR-148a-5p, and miR-139-5p) downregulated miRNAs (Figure 1B,C). The fold changes in miR-335-5p and miR-335-3p expression between the normal and AD samples were greater than those found for other miRNAs, and the fold change in miR-335-5p expression was similar to that found for miR-335-3p; thus we selected miR-335-5p for subsequent research. RT-qPCR assay further showed that miR-335-5p was significantly downregulated in the AD group compared with that in the normal group (Figure 1D). These data indicate that the miR-335-5p level is decreased in AD.

miR-335-5p mimic inhibits the proliferation, migration and phenotypic switching of HA-VSMCs induced by PDGF-BB

PDGF-BB can trigger the synthetic (dedifferentiated) phenotype, proliferation and migration of VSMCs and the participation of these

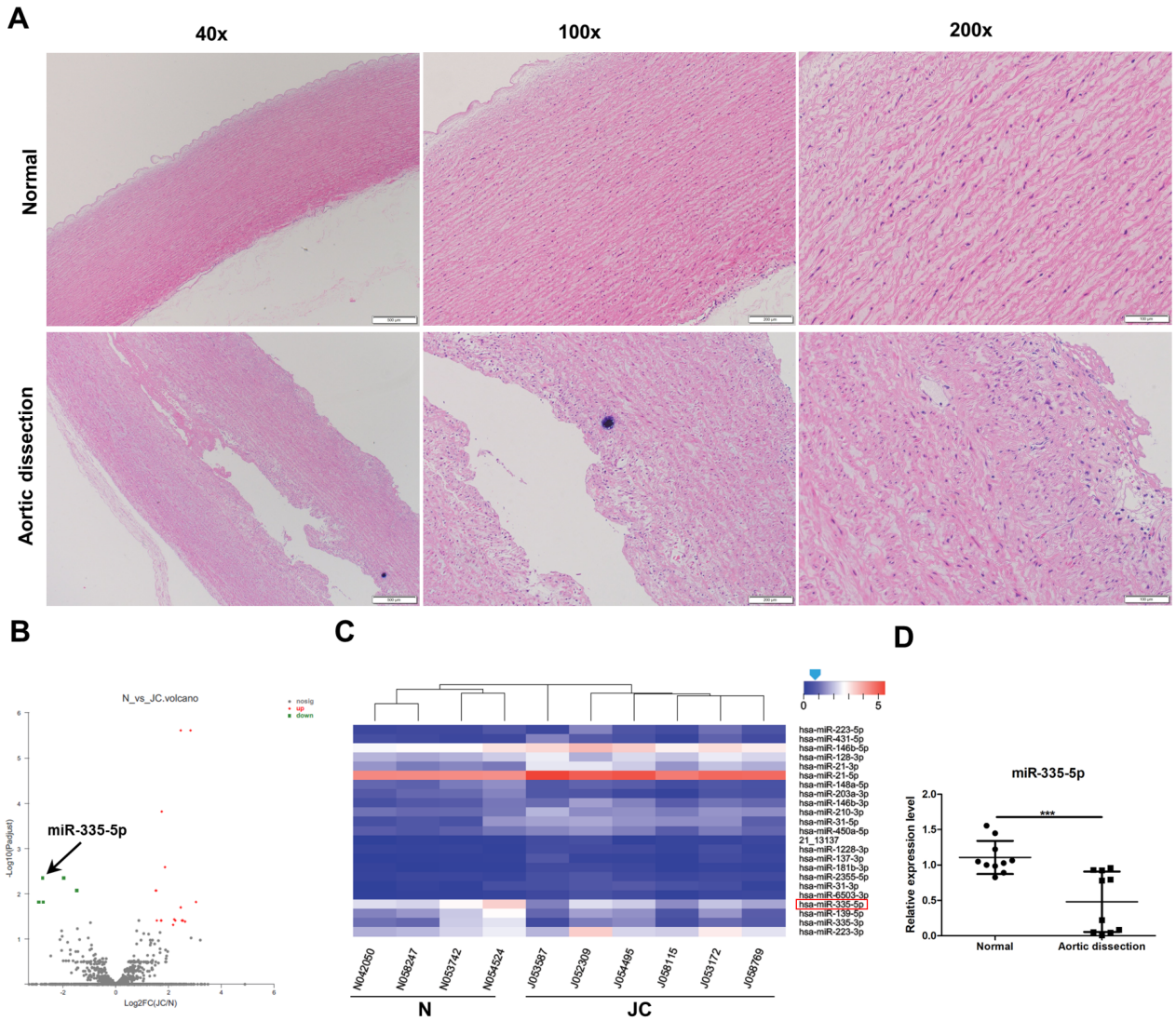

Figure 1. miR-335-5p is downregulated in human AD tissue (A) H&E staining of dissected aortic tissues and normal aortic tissues. The top row shows the normal group, and the bottom row shows the AD group. Scale bars: 500 μm (left), 200 μm (center) and 100 μm (right), $n = 5$. (B) Volcano map of the differentially expressed miRNAs between AD and normal tissues, which included 18 upregulated miRNAs (red) and 5 downregulated miRNAs (green). (C) Heatmap of differentially expressed miRNAs in the AD group compared with that in the normal group. N: normal tissues; JC: aortic dissection tissues. (D) The expression of miR-335-5p as validated by RT-qPCR. Data are expressed as the mean ± SD ($n = 10$) based on triplicate independent experiments and were analyzed by Student's *t*-test. $^{*}P < 0.05$, $^{**}P < 0.01$ and $^{***}P < 0.001$.

cells in vascular remodeling [39]. Therefore, PDGF-BB was used to establish the pathological HA-VSMC models. HA-VSMCs were exposed to PDGF-BB, and the expression of miR-335-5p was significantly lower in the PDGF-BB-treated cells than in the control cells (Figure 2A). HA-VSMCs were transfected with miR-335-5p mimic to overexpress miR-335-5p (Figure 2B). The CCK-8 and EdU assays revealed a significant decrease in cell proliferation after miR-335-5p treatment with or without PDGF-BB stimulation (Figure 2C, D). The miR-335-5p mimic markedly decreased the number of migrated cells both in the presence and in the absence of PDGF-BB (Figure 2E). The miR-335-5p mimic significantly inhibited the migration of VSMCs compared with that found in the NC group, regardless of induction with PDGF-BB (Figure 2F). Protuberance of the plasma membrane or extension of the lamellar pseudopod at the cell margin is the main driving force for HA-VSMC migration; thus cell migration is closely related to the polymerization, depolymerization and rearrangement of the actin cytoskeleton (F-actin) [40]. The F-actin formation analysis revealed a few irregular and scattered stress fiber bundles in the untreated HA-VSMCs, in contrast, a higher number of F-actin stress fibers were arranged longitudinally and parallel in the PDGF-BB-treated cells, and this effect was accompanied by reorganization of the actin cytoskeleton with the formation of lamellipodia. Moreover, the miR-335-5p mimic markedly suppressed the formation of migration-related F-actin stress fibers, and this structural change was associated with an increased cell size, as assessed by calculating the cell area (Figure 2G). These results revealed that miR-335-5p is a potential regulator of HA-VSMC proliferation and migration in the pathogenesis of AD.

To further demonstrate the impact of miR-335-5p on the phenotypic switching of HA-VSMCs, the expressions of various contractile mar-

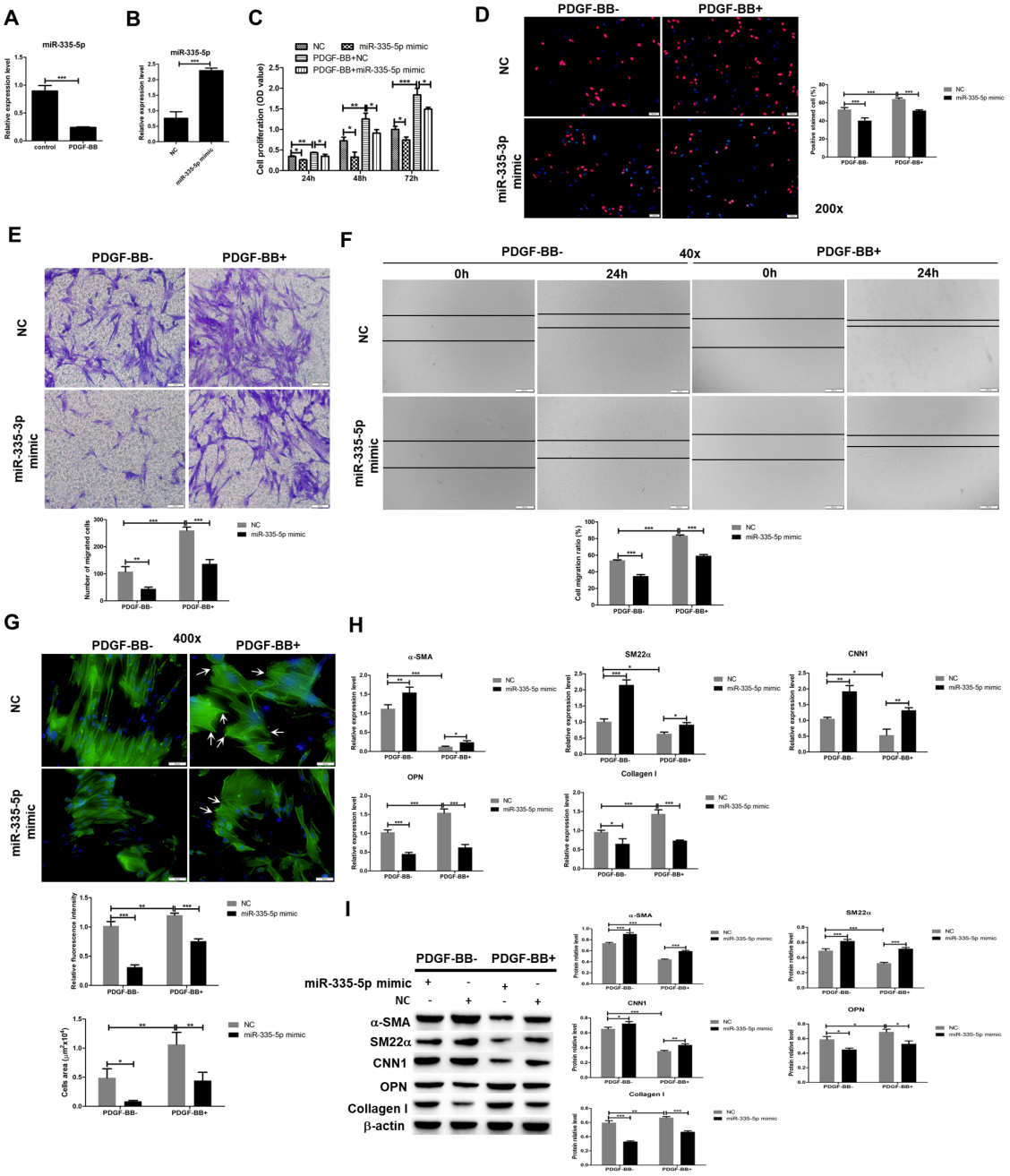

Figure 2. Role of miR-335-5p in the proliferation, migration and phenotypic switching of PDGF-BB-treated HA-VSMCs (A) The expression of miR-335-5p in HA-VSMCs treated or not treated with PDGF-BB was detected by RT-qPCR ($n=3$). (B) The overexpression efficiency of the miR-335-5p mimic was examined by RT-qPCR ($n=3$). (C) The proliferation of HA-VSMCs in the different groups at different time points was detected by the CCK-8 assay ($n=3$). (D) The proliferation rate was measured by the 5-ethynyl-2′-deoxyuridine (EdU) assay (left, scale bar = 50 μm), and the EdU-positive cell percentage was calculated (right, $n=3$). (E) Representative photographs of Transwell assays of the different groups (upper), scale bar = 100 μm, and quantitative analysis of the number of migrated cells (lower, $n=3$). (F) Representative images of the wound-healing assay of the different groups are shown (upper, scale bar = 500 μm), and the wound closure ratio was analyzed (lower, $n=3$). (G) Representative fluorescence microscopy images of F-actin stress fibers in HA-VSMCs of the different groups (upper). The white arrows denote lamellipodia. Green, stress fibers (F-actin); blue, DAPI. Scale bar = 50 μm. The mean optical density of F-actin expression in the different groups was quantified based on 6 visual fields using ImageJ 2x software ($n=3$). Quantitative analysis of the cell area ($n=3$). (H,I) The mRNA and protein levels of contractile and synthetic genes in HA-VSMCs of the different groups were analyzed by RT-qPCR and western blot analysis, respectively, $n=3$. Data are expressed as the mean ± SD based on triplicate independent experiments and were analyzed by one-way ANOVA. $^{*}P<0.05$, $^{**}P<0.01$ and $^{***}P<0.001$.

kers including α-SMA, SM22α and calponin (CNN1), and synthetic markers (OPN and Collagen I) of HA-VSMCs were determined by RT-qPCR and western blot analysis. As shown in Figure 2H,I, the miR-335-5p mimic significantly increased the expressions of SM22α, α-SMA and CNN1 in cells that were treated or not treated with PDGF-BB; moreover, decreased OPN and Collagen I expression was observed in

HA-VSMCs treated with the miR-335-5p mimic in the presence or absence of PDGF-BB. These findings support the notion that miR-335-5p is a novel regulator of the phenotypic switching of HA-VSMCs.

miR-335-5p suppresses AD progression *in vivo*

To demonstrate whether miR-335-5p represses vascular lesion formation *in vivo*, we constructed an AD mouse model with vascular media degeneration through administration of a peritoneal injection of angiotensin II and a high-fat diet for 4 weeks. As determined by H&E staining, VSMCs with a normal morphology and no vascular lesion formation were found in the control group; vascular media degeneration with larger and more rounded VSMCs, deficiency of the normal VSMC contractile apparatus, and dissection formation were observed in the AD model + Ad-NC group; and significant repression of aorta dilatation and a significantly reduced vascular media thickness were found in the AD model + Ad-miR-335-5p group (Figure 3A). To corroborate the *in vitro* results, we then detected the expressions of SP1, α-SMA and Collagen I, and found that the miR-335-5p-injected mice exhibited higher expressions of SP1 and α-SMA and a concomitant decrease in the Collagen I protein distribution (Figure 3B). These data suggest that miR-335-5p significantly suppresses vascular media degeneration by inhibiting SP1 during AD progression.

Identification of SP1 as a target gene of miR-335-5p in HA-VSMCs

TargetScan (http://targetscan.org/) was used to predict the target of miR-335-5p with the aim of exploring the potential mechanism of miR-335-5p in the PDGF-BB-induced phenotypic switching of HA-VSMCs. SP1 was found to be the target gene of miR-335-5p, and the putative binding site was found in the SP1 3′-UTR at 4578–4586, as shown in Figure 4A. Subsequently, two luciferase vectors containing the 100-bp WT or MUT 3′-UTR of SP1 were constructed and used in a luciferase reporter assay to confirm the predictions. HA-VSMCs were cotransfected with NC or miR-335-5p mimic and the psi-CHECK2, SP1-WT or SP1-MUT luciferase reporter vector. A dual-luciferase reporter assay revealed that the miR-335-5p mimic significantly suppressed the relative luciferase activity in HA-VSMCs transfected with SP1-WT, but significant suppression was not observed with SP1-MUT (Figure 4B). The RT-qPCR data revealed a negative correlation between miR-335-5p and SP1 expression (Figure 4C), and SP1 was upregulated in the aortic tissues of patients with AD (Figure 4D) and in HA-VSMCs treated with PDGF-BB (Figure 4E). The miR-335-5p mimic was transfected into HA-VSMCs

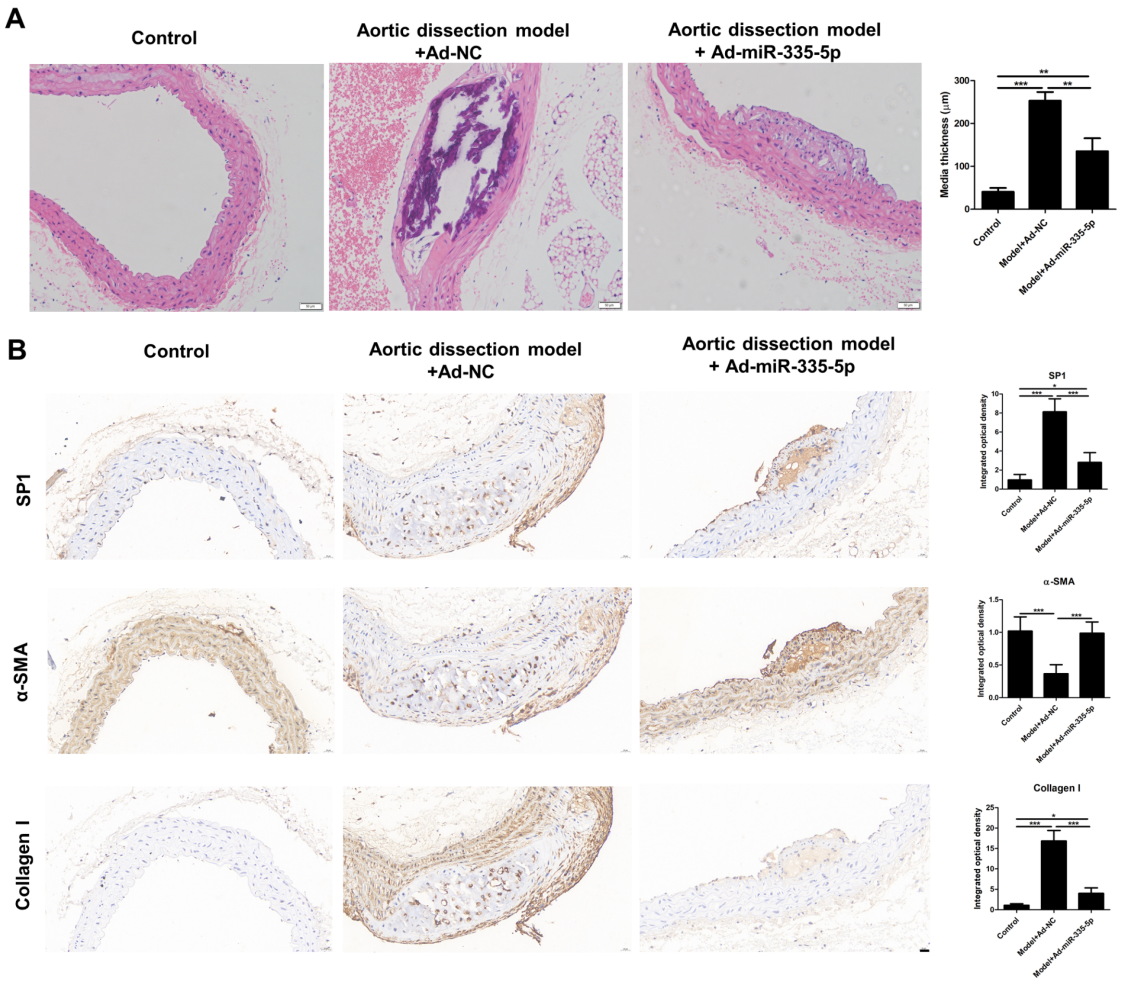

Figure 3. miR-335-5p inhibits dissection formation *in vivo* (A) Representative graphs of H&E-stained aortas from the different groups. Data are presented as the mean ± SD. Scale bar = 50 μm. Quantitative analysis of the aortic media thickness of the different groups. (B) SP1, α-SMA, and Collagen I staining based on an immunohistochemistry assay and quantification of cells positive for these markers ($n = 5$). Scale bar = 20 μm. Data are expressed as the mean ± SD based on triplicate independent experiments and were analyzed by one-way ANOVA. $^{*}P < 0.05$, $^{**}P < 0.01$ and $^{***}P < 0.001$.

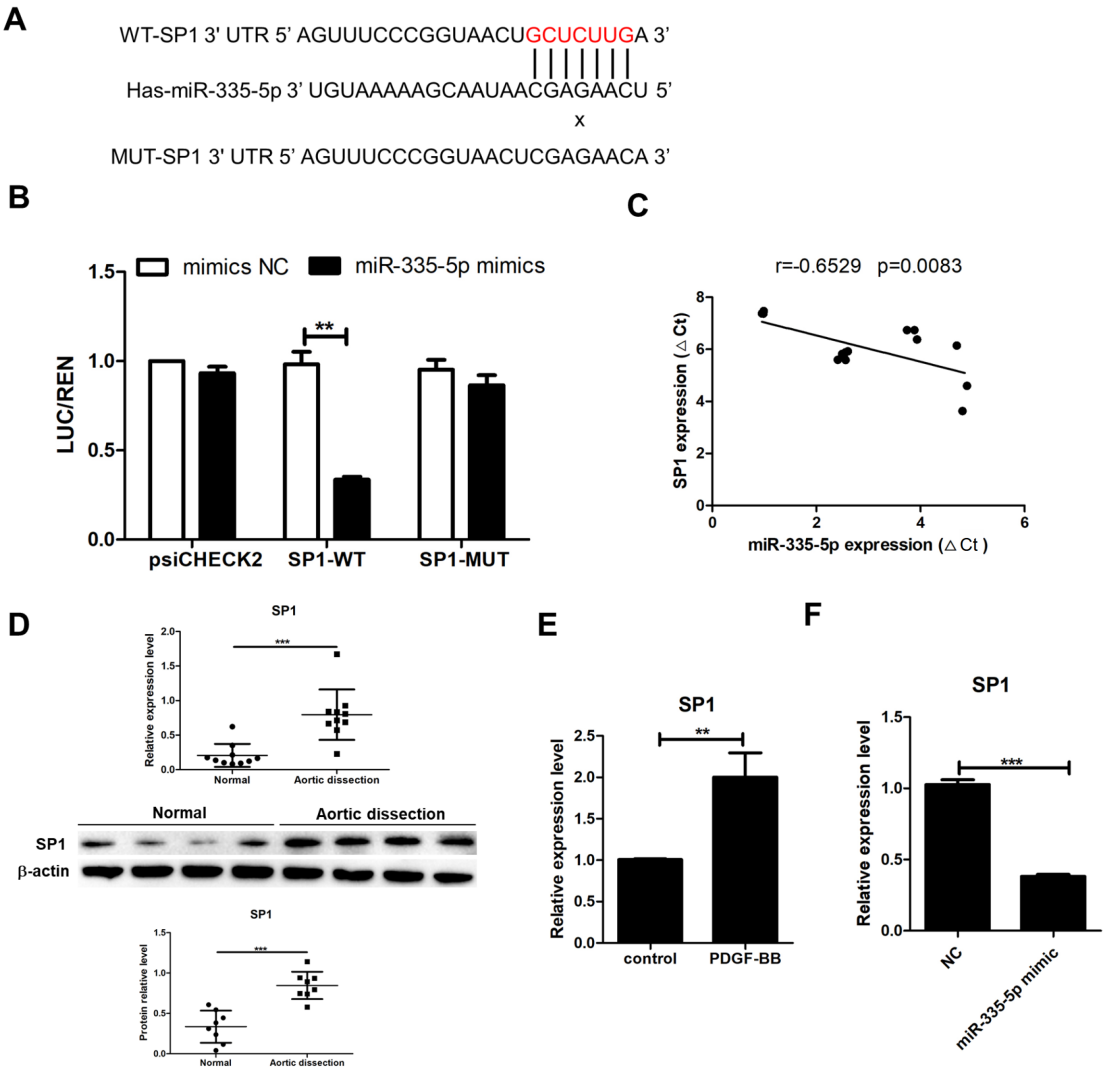

Figure 4. SP1 is a target of miR-335-5p (A) Theoretical sequence alignment of miR-335-5p and the 3′-UTR of SP1 predicted using TargetScan. (B) Luciferase assay of HA-VSMCs. The relative luciferase activities (normalized to Renilla luciferase activities) of plasmids carrying WT/MUT SP1 were analyzed ($n=3$). (C) The correlation between the miR-335-5p and SP1 levels in AD was measured based on a Pearson correlation analysis ($n=15$). (D–F) The mRNA and protein levels of SP1 in AD tissues, PDGF-BB-treated HA-VSMCs ($n=3$) and miR-335-5p mimic-transfected HA-VSMCs ($n=3$) were detected by RT-qPCR (upper, $n=10$) and western blot analysis (middle and lower, $n=8$). Data are expressed as the mean ± SD based on triplicate independent experiments and were analyzed by one-way ANOVA. $^{**}P<0.01$ and $^{***}P<0.001$.

to further confirm whether SP1 is directly regulated by miR-335-5p. The RT-qPCR data revealed that SP1 was markedly downregulated after transfection with the miR-335-5p mimic (Figure 4F). These results showed that the expression of SP1 is regulated by miR-335-5p, which indicates that miR-335-5p regulates AD progression by targeting SP1.

SP1 downregulation inhibits HA-VSMC proliferation, migration and phenotypic switching

To further investigate the impact of SP1 on HA-VSMC function, we inserted the SP1 shRNA sequence into the pGPH1/Neo plasmid, and the SP1 shRNA plasmid was then transfected into HA-VSMCs treated or not treated with PDGF-BB to detect the proliferation, migration and phenotypic switching of HA-VSMCs by CCK-8, Transwell, wound-healing and RT-qPCR assays. As presented in Figure 5A, HA-VSMCs were transfected with SP1 shRNA to downregulate SP1. The CCK-8 assay revealed a significant decrease in cell proliferation after SP1 shRNA treatment with or without PDGF-BB stimulation (Figure 5B). The Transwell and wound-healing assays showed that SP1 shRNA significantly inhibited HA-VSMC migration and that PDGF-BB treatment promoted cell migration (Figure 5C,D). In addition, the RT-qPCR data suggested that SP1 shRNA markedly increased the expressions of contractile markers (α-SMA, SM22α and CNN1) and inhibited the expression of synthetic markers (OPN and Collagen I) regardless of PDGF-BB stimulation (Figure 5E). Taken together, these data confirm that SP1 is an important mediator of HA-VSMC proliferation, migration and phenotypic switching and that SP1 is associated with the miR-335-5p-mediated regulation of HA-VSMC function.

miR-335-5p alleviates PDGF-BB-induced HA-VSMC proliferation, migration and phenotypic switching through the modulation of SP1 expression

To demonstrate the biological function of miR-335-5p mediated by

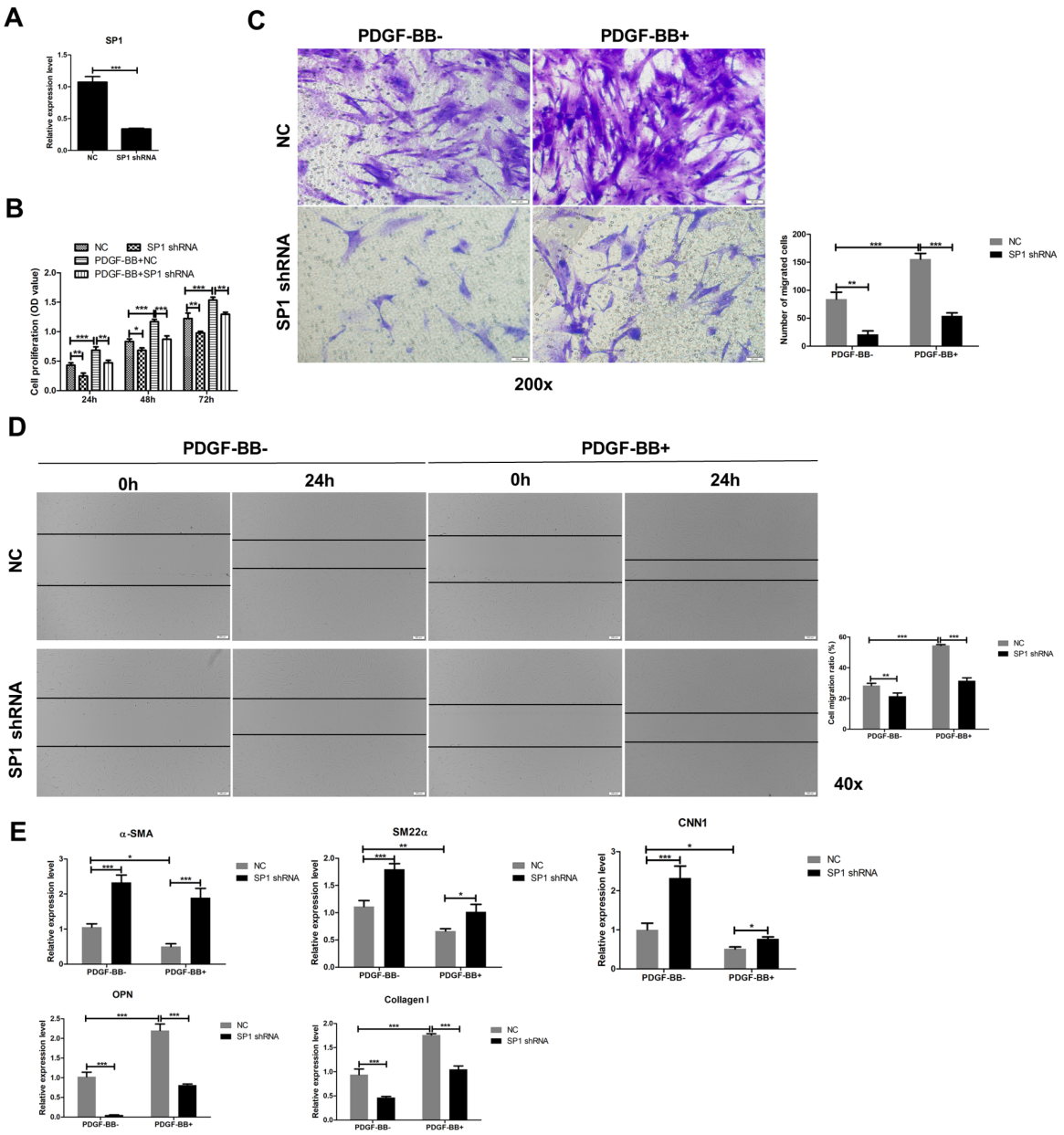

Figure 5. SP1 is involved in HA-VSMC proliferation, migration and phenotypic switching (A) The transfection efficiency of SP1/pGPH1 was examined by RT-qPCR ($n = 3$). (B) The proliferation of HA-VSMCs in the different groups at different times was detected by the CCK-8 assay ($n = 3$). (C) Representative images of Transwell assay of the different groups (upper, scale bar = 50 μm), and quantitative analysis of the number of migrated cells (lower, $n = 3$). (D) Representative images of the wound-healing assay of the different groups (left, scale bar = 200 μm) are shown, and the wound closure ratio was analyzed (right, $n = 3$). (E) RT-qPCR analysis of the mRNA expression levels of contractile markers (α-SMA, SM22α, and CNN1) and synthetic markers (OPN and Collagen I) in the different groups ($n = 3$). Data are expressed as the mean ± SD based on triplicate independent experiments and were analyzed by one-way ANOVA. $^{*}P < 0.05$, $^{**}P < 0.01$ and $^{***}P < 0.001$.

SP1 in AD progression, functional rescue assays were designed with HA-VSMCs. As shown in Figure 6A, in the presence of PDGF-BB, the decrease in cell proliferation induced by the miR-335-5p mimic showed recovery with the simultaneous transfection with SP1/pcDNA3.1 and was aggravated by the simultaneous transfection with SP1/pGPH1. Moreover, the miR-335-5p-induced inhibition of migration and the observed decreases in the F-actin levels and cell areas were reversed by the simultaneous transfection with SP1/pcDNA3.1, and all of these effects were aggravated by the simultaneous transfection with SP1/pGPH1 (Figure 6B–F). Importantly, in the presence of PDGF-BB, many HA-VSMCs exhibited reorganization of the actin cytoskeleton with the formation of lamellipodia, which was consistent with a migratory cell phenotype, and the decrease in migratory HA-VSMCs induced by the miR-335-5p mimic could be rescued by the simultaneous overexpression of SP1 and aggravated by the simultaneous knockdown of SP1 (Figure 6F). We also confirmed that the miR-335-5p mimic promoted the expressions of several contractile genes (SM22α, CNN1) and reduced the expressions of synthetic gene (OPN) at both the mRNA level (Figure 6G) and the protein level (Figure 6H) in the presence of

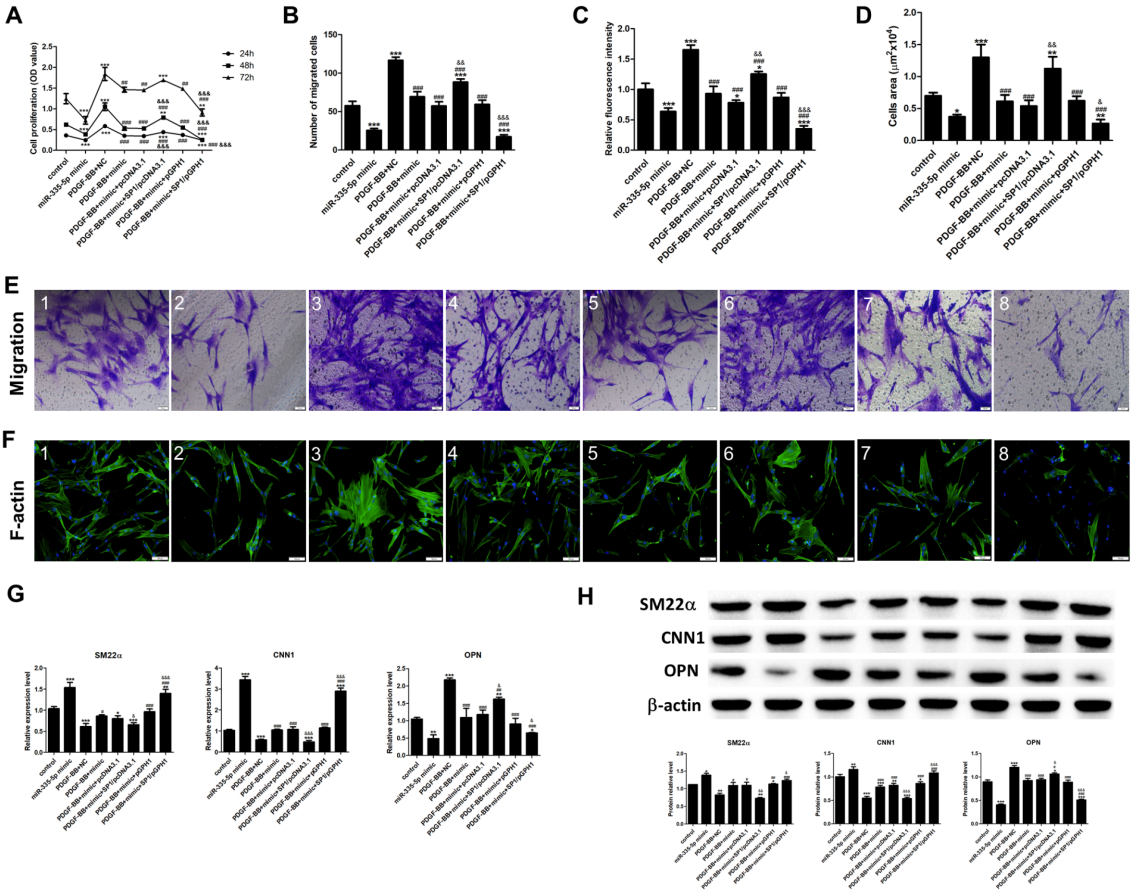

Figure 6. miR-335-5p upregulates HA-VSMC proliferation, migration and phenotypic switching by targeting SP1 (A) The proliferation of HA-VSMCs in the different groups at different times was detected by the CCK-8 assay ($n = 3$). (B) Quantitative analysis of the number of migrated cells in the Transwell assay ($n = 3$). (C) The mean optical density of F-actin expression in the different groups was analyzed based on 6 visual fields using ImageJ 2x software, and the relative fluorescence intensity was calculated ($n = 3$). (D) Quantitative analysis of the cell area ($n = 3$). (E) Representative images of Transwell assays of the different groups. Scale bar = 50 μm. (F) Representative fluorescence microscopy images of stress fiber F-actin in HA-VSMCs of the different groups. Green, stress fibers (F-actin); blue, DAPI. Scale bar = 100 μm. (G) The phenotypic switching of HA-VSMCs was determined by western blot analysis. (H) Quantitative results of the western blot analysis, $n = 3$. Data are expressed as the mean ± SD based on triplicate independent experiments and were analyzed by one-way ANOVA. $^{*}P < 0.05$, $^{**}P < 0.01$ and $^{***}P < 0.001$ vs the control group; $^{\#}P < 0.05$, $^{\#\#}P < 0.01$ and $^{\#\#\#}P < 0.001$ vs the PDGF-BB + NC group; $^{\&}P < 0.05$, $^{\&\&}P < 0.01$ and $^{\&\&\&}P < 0.001$ vs the PDGF-BB + miR-335-5p mimic group. 1: the control group; 2: the miR-335-5p mimic group; 3: the PDGF-BB + NC group; 4: the PDGF-BB + mimic group; 5: the PDGF-BB + mimic + pcDNA3.1 group; 6: the PDGF-BB + mimic + SP1/pcDNA3.1 group; 7: the PDGF-BB + mimic + pGPH1 group; 8: the PDGF-BB + mimic + SP1/pGPH1 group.

PDGF-BB, and these effects were inhibited by the simultaneous transfection with SP1/pcDNA3.1 and promoted by the simultaneous transfection with SP1/pGPH1. These results confirm that the function of miR-335-5p in inhibiting the proliferation, migration and phenotypic switching of HA-VSMCs is achieved by the negative regulation of SP1 expression.

Discussion

AD is a life-threatening medical emergency with very high mortality [41,42]. Previous studies on the pathogenesis of AD focused on the degeneration of the aortic media, the phenotypic switching of smooth muscle cells, the inflammatory process of the aortic media and the degradation mechanism of the extracellular matrix [43,44]. VSMCs, as the main cellular component of the aortic media [10], have long been the focus of research on the pathogenesis of AD. VSMCs exhibit two types of phenotypes: contractile and synthetic. The VSMCs found in normal aortas mainly exhibit a contractile phenotype, which is characterized by a high differentiation degree, low proliferation and migration abilities, and strong contractile ability. However, the VSMCs in AD are mainly synthetic and thus exhibit low differentiation, enhanced proliferation and migration abilities, and weak contractile ability [45].

Our miRNA-seq data revealed that 18 miRNAs (such as miR-21-5p, miR-210-3p and miR-31-5p) were upregulated and 5 miRNAs (miR-203a-3p, miR-335-5p, miR-148a-5p, miR-335-3p and miR-139-5p) were downregulated in the AD group compared with those in the normal group. A previous study showed that miR-31-5p exaggerates VSMC phenotypic switching *in vitro* and promotes aortic aneurysm/dissection development *in vivo* [46]. Our miRNA-seq data also indicated the probable and potential positive regulatory effects on AD. To our knowledge, the participation of miR-335-5p in aortic diseases has not been previously investigated. Many studies have demonstrated that miR-335 is involved in the progression of acute myeloid leukemia, ovarian cancer and colorectal liver metastases [27–29]. Moreover, miR-335 may be a potential therapeutic target in cardiac fibrosis and hypertrophy [25]. However, the effect of miR-335-5p on VSMC phenotype switching during the development of AD has not been clarified. In the present study, through an

RT-qPCR analysis of aortic tissues from normal individuals and patients with AD, we first found that AD aortic tissues had low miR-335-5p expression and high SP1 expression, and demonstrated that miR-335-5p might play a role in the pathophysiologic processes of AD by regulating SP1. Our data showed that miR-335-5p inhibited PDGF-BB-induced VSMC proliferation, migration and phenotypic switching via SP1. Yuan *et al.* [14] and Yan *et al.* [15] found that VSMCs undergo switching from the contractile to the synthetic phenotype and play a role in AD.

PDGF-BB, which is derived from platelets, endothelial cells and macrophages, exerts chemotactic effects, stimulates the proliferation and migration of smooth muscle cells and is a chemotactic agent *in vitro* [39]. This potent atherogenic stimulus also triggers VSMC dedifferentiation, proliferation, and migration into the neointima after artery injury [47,48]. Therefore, to investigate the effect of miR-335-5p on VSMC proliferation and migration, gain-of-function experiments were performed using cells treated with PDGF-BB. We found that the expression of miR-335-5p in PDGF-BB-treated cells was lower than that in NC-treated cells. Moreover, miR-335-5p upregulation significantly inhibited human VSMC proliferation and migration. Our mechanistic analysis confirmed that the transcription factor SP1 is a pivotal target of miR-335-5p in VSMCs. SP1, which is a member of the SP1/Krüppel-like transcription factor family [49], is involved in the development and progression of cardiovascular diseases by promoting the proliferation and migration of VSMCs [50,51]. Our results demonstrated that SP1 silencing significantly inhibited human VSMC proliferation and migration. A previous study proved that SP1 is upregulated following vascular injury *in vivo* and that SP1 knockdown abolishes the PDGF-BB-induced switching of VSMCs from the contractile to the synthetic phenotype [52]. Our gain-of-function and loss-of-function experimental data for SP1 also support and confirm this notion. We further demonstrated that miR-335-5p suppresses PDGF-BB-induced VSMC proliferation and migration via the target gene SP1. Angiotensin II can cause elevated blood pressure, and long-term hypertension can lead to intimal hyperplasia of the aorta, which in turn leads to intimal injury of the aorta, tearing of the medial membrane, and dissection [53]. Furthermore, the overexpression of miR-335-5p in mouse models of AD induced by angiotensin II clearly suppressed vascular media degeneration and dissection formation.

The regulation of the VSMC phenotype is important in vascular remodeling and lesion formation [10], and VSMC phenotypic switching plays a crucial role in AD [54]. Patients with AD exhibit lower expressions of SM22α, α-SMA and MHC in contractile smooth muscle cells and higher expressions of vimentin and OPN in synthetic smooth muscle cells in the aortic wall compared with normal individuals [55]. The characteristic biological change during the initiation and development of AD is the transformation of VSMCs from the contractile to the synthetic type, and related genes can be used as a reference for the prediction of AD [55]. OPN, as a new cytokine, shows high expression in the arterial wall tissue of patients with thoracic AD [16], which suggests that OPN plays an important role in AD. Yuan *et al.* [56] indicated that the upregulation of OPN may play a role in the pathogenesis of aortopathies, including AD, aortic aneurysm, and coronary artery disease. In cardiovascular diseases, the phenotype of VSMCs is altered, and the expressions of the abovementioned specific VSMC biomarkers are modulated [10]. Collagen I is also regarded as a synthetic VSMC marker in VSMC phenotypic switching [57,58]. In the current study, we evaluated the impact of miR-335-5p on the phenotypic switching of VSMCs and found that high levels of miR-335-5p reduced the expressions of the synthetic markers OPN and Collagen I and increased the levels of the contractile markers α-SMA, SM22α and CNN1. Moreover, SP1 was confirmed to serve as a mediator of the effect of miR-335-5p on the phenotypic switching of VSMCs. Many studies have observed low expression of miR-335-5p in breast cancer, lung cancer and stomach cancer, and this low expression of miR-335-5p results in loss of its regulatory effect on the target gene, which leads to the promotion of initiation and development of tumors [59–61]. However, whether miR-335-5p can inhibit the development of AD by negatively regulating SP1 has not been reported.

In summary, our study showed that aortic specimens from patients with AD presented higher level of miR-335-5p than those from normal controls. The upregulation of miR-335-5p inhibited VSMC proliferation and migration and induced VSMC phenotypic switching from the synthetic to the contractile type by directly downregulating SP1 *in vitro*. Thus, miR-335-5p/SP1 signaling might be a novel therapeutic target for the treatment of AD. Our results demonstrate the potential of applying miR-335-5p as a therapeutic strategy for cardiovascular diseases characterized by VSMC proliferation, and indicate that miR-335-5p/SP1 signaling may occur in VSMCs through a mechanism that needs to be further investigated.

Funding

This work was supported by the grants from the Open Project of the State Key Laboratory of Cardiovascular Diseases (No. 2019kfyf-05) and the Association Foundation Program of Yunnan Provincial Science and Technology Department and Kunming Medical University (Nos. 202001AY070001-106 and 202001AY070001-009)

Conflict of Interest

The authors declare that they have no conflict of interest.

References

1. Ito T, Yasuda N, Kuroda Y, Sugawara M, Koyanagi T, Higami T. Acute gallbladder necrosis in a patient with acute type B aortic dissection. *Ann Vascular Dis* 2013, 6: 748–750
2. Isoda S, Osako M, Kimura T, Mashiko Y, Yamanaka N, Nakamura S, Maehara T. Coronary malperfusion due to flap suffocation after acute type A dissection surgery. *Ann Thorac Cardiovasc Surg* 2012, 18: 144–147
3. Kitamura T, Kigawa I, Fukuda S, Miyairi T, Takamoto S. Long term results with the Cabrol aortic root replacement. *Int Heart J* 2011, 52: 229–232
4. Thompson RW. Detection and management of small aortic aneurysms. *N Engl J Med* 2002, 346: 1484–1486
5. Apostolakis E, Akinosoglou K. What's new in the biochemical diagnosis of acute aortic dissection: problems and perspectives. *Med Sci Monit* 2007, 13: RA154–158
6. Choi JC, LeMaire SA. Thoracic aortic dissection: genes, molecules, and the knife. *Tex Heart Inst J* 2012, 39: 838–839
7. Tian XL, Li Y. Endothelial cell senescence and age-related vascular diseases. *J Genet Genomics* 2014, 41: 485–495
8. Lv SJ, Ding YN, Pei XY, Zhao X, Hao DL, Zhang ZQ, Chen HZ, *et al.* Vascular transcriptome profiling reveals aging-related genes in angiotensin II-induced hypertensive mouse aortas. *Chin Med Sci J* 2020, 35: 43–53
9. Li Y, Yan H, Guo J, Han Y, Zhang C, Liu X, Du J, *et al.* Down-regulated

RGS5 by genetic variants impairs endothelial cell function and contributes to coronary artery disease. *Cardiovasc Res* 2021, 117: 240–255
10. Owens GK, Kumar MS, Wamhoff BR. Molecular regulation of vascular smooth muscle cell differentiation in development and disease. *Physiol Rev* 2004, 84: 767–801
11. Beneit N, Fernández-García CE, Martín-Ventura JL, Perdomo L, Escribano Ó, Michel JB, García-Gómez G, ***et al.*** Expression of insulin receptor (IR) A and B isoforms, IGF-IR, and IR/IGF-IR hybrid receptors in vascular smooth muscle cells and their role in cell migration in atherosclerosis. *Cardiovasc Diabetol* 2016, 15: 161
12. Alexander MR, Owens GK. Epigenetic control of smooth muscle cell differentiation and phenotypic switching in vascular development and disease. *Annu Rev Physiol* 2012, 74: 13–40
13. Wang D, Uhrin P, Mocan A, Waltenberger B, Breuss JM, Tewari D, Mihaly-Bison J, ***et al.*** Vascular smooth muscle cell proliferation as a therapeutic target. Part 1: molecular targets and pathways. *Biotechnol Adv* 2018, 36: 1586–1607
14. Yuan Y, Wang C, Xu J, Tao J, Xu Z, Huang S. BRG1 overexpression in smooth muscle cells promotes the development of thoracic aortic dissection. *BMC Cardiovasc Disord* 2014, 14: 144
15. Yan Y, Tan MW, Xue X, Ding XY, Wang GK, Xu ZY. Involvement of Oct4 in the pathogenesis of thoracic aortic dissection via inducing the dedifferentiated phenotype of human aortic smooth muscle cells by directly upregulating KLF5. *J Thoracic Cardiovasc Surg* 2016, 152: 820–829.e4
16. Wang L, Zhang J, Fu W, Guo D, Jiang J, Wang Y. Association of smooth muscle cell phenotypes with extracellular matrix disorders in thoracic aortic dissection. *J Vascular Surg* 2012, 56: 1698–1709.e1
17. Lytle JR, Yario TA, Steitz JA. Target mRNAs are repressed as efficiently by microRNA-binding sites in the 5′ UTR as in the 3′ UTR. *Proc Natl Acad Sci USA* 2007, 104: 9667–9672
18. Moreno-Moya JM, Vilella F, Simón C. MicroRNA: key gene expression regulators. *Fertil Steril* 2014, 101: 1516–1523
19. Wilczynska A, Bushell M. The complexity of miRNA-mediated repression. *Cell Death Differ* 2015, 22: 22–33
20. Filipowicz W, Bhattacharyya SN, Sonenberg N. Mechanisms of post-transcriptional regulation by microRNAs: are the answers in sight? *Nat Rev Genet* 2008, 9: 102–114
21. Wang XJ, Huang B, Yang YM, Zhang L, Su WJ, Tian L, Lu TY, ***et al.*** Differential expression of microRNAs in aortic tissue and plasma in patients with acute aortic dissection. *J Geriatr Cardiol* 2015, 12: 655–661.
22. Xu Z, Wang Q, Pan J, Sheng X, Hou D, Chong H, Wei Z, ***et al.*** Characterization of serum miRNAs as molecular biomarkers for acute Stanford type A aortic dissection diagnosis. *Sci Rep* 2017, 7: 13659
23. Wang L, Zhang S, Xu Z, Zhang J, Li L, Zhao G. The diagnostic value of microRNA-4787-5p and microRNA-4306 in patients with acute aortic dissection. *Am J Transl Res* 2017, 9: 5138–5149.
24. Pan Q, Li B, Zhang J, Du X, Gu D. LncRNA THAP9-AS1 accelerates cell growth of esophageal squamous cell carcinoma through sponging miR-335–5p to regulate SGMS2. *Pathol Res Pract* 2021, 224: 153526
25. Li M, Qi C, Song R, Xiong C, Zhong X, Song Z, Ning Z, ***et al.*** Inhibition of long noncoding RNA *SNHG20* improves angiotensin II-induced cardiac fibrosis and hypertrophy by regulating the microRNA 335/*Galectin-3* axis. *Mol Cell Biol* 2021, 41: e0058020
26. Oliveira SR, Dionísio PA, Gaspar MM, Correia Guedes L, Coelho M, Rosa MM, Ferreira JJ, ***et al.*** miR-335 targets LRRK2 and mitigates inflammation in Parkinson's disease. *Front Cell Dev Biol* 2021, 9: 661461
27. Zhang L, Wang X, Wu J, Xiao R, Liu J. MiR-335-3p inhibits cell proliferation and induces cell cycle arrest and apoptosis in acute myeloid leukemia by targeting EIF3E. *Biosci Biotechnol Biochem* 2021, 85: 1953–1961
28. Meng Q, Wang N, Duan G. Long non-coding RNA XIST regulates ovarian cancer progression via modulating miR-335/BCL2L2 axis. *World J Surg Onc* 2021, 19: 165
29. Lu C, Luo X, Xing C, Mao Y, Xu Y, Gao W, Wang W, ***et al.*** Construction of a novel mRNA-miRNA-lncRNA network and identification of potential regulatory axis associated with prognosis in colorectal cancer liver metastases. *Aging* 2021, 13: 14968–14988
30. Dynan WS, Tjian R. Isolation of transcription factors that discriminate between different promoters recognized by RNA polymerase II. *Cell* 1983, 32: 669–680
31. Nam EH, Lee Y, Zhao XF, Park YK, Lee JW, Kim S. ZEB2–Sp1 cooperation induces invasion by upregulating cadherin-11 and integrin α5 expression. *Carcinogenesis* 2014, 35: 302–314
32. Beishline K, Azizkhan-Clifford J. Sp1 and the 'hallmarks of cancer'. *FEBS J* 2015, 282: 224–258
33. Chen SJ, Wu P, Sun LJ, Zhou B, Niu W, Liu S, Lin FJ, ***et al.*** miR-204 regulates epithelial-mesenchymal transition by targeting SP1 in the tubular epithelial cells after acute kidney injury induced by ischemia-reperfusion. *Oncol Rep* 2017, 37: 1148–1158
34. Li Y, Feng D, Wang Z, Zhao Y, Sun R, Tian D, Liu D, ***et al.*** Ischemia-induced ACSL4 activation contributes to ferroptosis-mediated tissue injury in intestinal ischemia/reperfusion. *Cell Death Differ* 2019, 26: 2284–2299
35. Cai LJ, Tu L, Li T, Yang XL, Ren YP, Gu R, Zhang Q, ***et al.*** Up-regulation of microRNA-375 ameliorates the damage of dopaminergic neurons, reduces oxidative stress and inflammation in Parkinson's disease by inhibiting SP1. *Aging* 2020, 12: 672–689
36. Wang R, Yang Y, Wang H, He Y, Li C. MiR-29c protects against inflammation and apoptosis in Parkinson's disease model *in vivo* and *in vitro* by targeting SP1. *Clin Exp Pharmacol Physiol* 2020, 47: 372–382
37. Ramanan VK, Saykin AJ. Pathways to neurodegeneration: mechanistic insights from GWAS in Alzheimer's disease, Parkinson's disease, and related disorders. *Am J Neurodegener Dis* 2013, 2: 145–175
38. Tang Y, Yu S, Liu Y, Zhang J, Han L, Xu Z. MicroRNA-124 controls human vascular smooth muscle cell phenotypic switch via Sp1. *Am J Physiol Heart Circ Physiol* 2017, 313: H641–H649
39. Jawien A, Bowen-Pope DF, Lindner V, Schwartz SM, Clowes AW. Platelet-derived growth factor promotes smooth muscle migration and intimal thickening in a rat model of balloon angioplasty. *J Clin Invest* 1992, 89: 507–511
40. Webb DJ, Parsons JT, Horwitz AF. Adhesion assembly, disassembly and turnover in migrating cells—over and over and over again. *Nat Cell Biol* 2002, 4: E97–E100
41. Chen LW, Wu XJ, Dai XF, Liao DS, Li C, Wang QM, Dong Y. A self-adaptive triple-branched stent graft for arch repair during open type A dissection surgery. *J Thoracic Cardiovasc Surg* 2015, 149: 1278–1283.e1
42. Zhu JM, Qi RD, Chen L, Liu W, Li CN, Fan ZM, Sun LZ. Surgery for acute type A dissection using total arch replacement combined with stented elephant trunk implantation: preservation of autologous brachiocephalic vessels. *J Thoracic Cardiovasc Surg* 2015, 150: 101–105
43. Karimi A, Milewicz DM. Structure of the elastin-contractile units in the thoracic aorta and how genes that cause thoracic aortic aneurysms and dissections disrupt this structure. *Canadian J Cardiol* 2016, 32: 26–34
44. Wang X, LeMaire SA, Chen L, Shen YH, Gan Y, Bartsch H, Carter SA, ***et al.*** Increased collagen deposition and elevated expression of connective tissue growth factor in human thoracic aortic dissection. *Circulation* 2006, 114:
45. Zhu SB, Zhu J, Zhou ZZ, Xi EP, Wang RP, Zhang Y. TGF-β1 induces human aortic vascular smooth muscle cell phenotype switch through PI3K/AKT/ID2 signaling. *Am J Transl Res* 2015, 7: 2764–2774

46. Yang K, Ren J, Li X, Wang Z, Xue L, Cui S, Sang W, *et al.* Prevention of aortic dissection and aneurysm via an ALDH2-mediated switch in vascular smooth muscle cell phenotype. *Eur Heart J* 2020, 41: 2442–2453
47. Tallquist M, Kazlauskas A. PDGF signaling in cells and mice. *Cytokine Growth Factor Rev* 2004, 15: 205–213
48. Liu B, Zhang JN, Pu PY. Expressions of PDGF-B and collagen type III in the remodeling of experimental saccular aneurysm in rats. *Neurol Res* 2008, 30: 632–638
49. Chu S. Transcriptional regulation by post-transcriptional modification—role of phosphorylation in Sp1 transcriptional activity. *Gene* 2012, 508: 1–8
50. Azahri NSM, Di Bartolo BA, Khachigian LM, Kavurma MM. Sp1, acetylated histone-3 and p300 regulate TRAIL transcription: mechanisms of PDGF-BB-mediated VSMC proliferation and migration. *J Cell Biochem* 2012, 113: 2597–2606
51. Yang HM, Kim BK, Kim JY, Kwon YW, Jin S, Lee JE, Cho HJ, *et al.* PPARγ modulates vascular smooth muscle cell phenotype via a protein kinase G-dependent pathway and reduces neointimal hyperplasia after vascular injury. *Exp Mol Med* 2013, 45: e65
52. Deaton RA, Gan Q, Owens GK. Sp1-dependent activation of KLF4 is required for PDGF-BB-induced phenotypic modulation of smooth muscle. *Am J Physiol-Heart Circulatory Physiol* 2009, 296: H1027–H1037
53. Khan IA, Nair CK. Clinical, diagnostic, and management perspectives of aortic dissection. *Chest* 2002, 122: 311–328
54. Zhang J, Wang L, Fu W, Wang C, Guo D, Jiang J, Wang Y. Smooth muscle cell phenotypic diversity between dissected and unaffected thoracic aortic media. *J Cardiovasc Surg (Torino)* 2013, 54: 511–521
55. An Z, Liu Y, Song ZG, Tang H, Yuan Y, Xu ZY. Mechanisms of aortic dissection smooth muscle cell phenotype switch. *J Thoracic Cardiovasc Surg* 2017, 154: 1511–1521.e6
56. Yuan SM, Wang J, Huang HR, Jing H. Osteopontin expression and its possible functions in the aortic disorders and coronary artery disease. *Rev Bras Cir Cardiovasc* 2011, 26: 173–182
57. Wang H, Jiang M, Xu Z, Huang H, Gong P, Zhu H, Ruan C. miR-146b-5p promotes VSMC proliferation and migration. *Int J Clin Exp Pathol* 2015, 8: 12901–12907
58. Yang L, Gao L, Nickel T, Yang J, Zhou J, Gilbertsen A, Geng Z, *et al.* Lactate promotes synthetic phenotype in vascular smooth muscle cells. *Circ Res* 2017, 121: 1251–1262
59. Heyn H, Engelmann M, Schreek S, Ahrens P, Lehmann U, Kreipe H, Schlegelberger B, *et al.* MicroRNA miR-335 is crucial for the BRCA1 regulatory cascade in breast cancer development. *Int J Cancer* 2011, 129: 2797–2806
60. Wang H, Li M, Zhang R, Wang Y, Zang W, Ma Y, Zhao G, *et al.* Effect of miR-335 upregulation on the apoptosis and invasion of lung cancer cell A549 and H1299. *Tumor Biol* 2013, 34: 3101–3109
61. Xu Y, Zhao F, Wang Z, Song Y, Luo Y, Zhang X, Jiang L, *et al.* MicroRNA-335 acts as a metastasis suppressor in gastric cancer by targeting Bcl-w and specificity protein 1. *Oncogene* 2012, 31: 1398–1407